

Rational design of hierarchically micrometer scaled macro-mesoporous ceria-zirconia composites for enhancing diesel soot catalytic combustion performance

Zhengzheng Yang^{a,*}, Zhi Chen^a, Yumeng Huang^a, Na Zhang^a, Yunxiang Li^a, Huangwei Zhang^{b,c,*}

^a College of Environmental Science and Engineering, China West Normal University, Nanchong, 637009, China

^b Advanced Manufacturing and Materials Centre, National University of Singapore Chongqing Research Institute, Chongqing 401123, China

^c Department of Mechanical Engineering, National University of Singapore, 9 Engineering Drive 1, 117576, Singapore

ARTICLE INFO

Keywords:

Soot catalytic oxidation
Catalyzed diesel particulate filter
Particulate matter purification
Soot-catalyst contact efficiency
macro-mesoporous CeO₂-ZrO₂

ABSTRACT

Diesel soot particulate is the primary source of urban atmospheric fine particulate matters (PM_{2.5}), catalytic soot elimination on diesel particulate filter is invariably an important yet challenging subject, because of the inherently poor solid-solid contact of soot-catalyst. In this study, we report a hierarchically porous ceria-zirconia composite with micrometer scaled macroporous structure, CZ-8, for enhancing catalyst-soot contact efficiency and soot catalytic combustion performance. Scanning electron microscope (SEM), N₂ adsorption-desorption and mercury porosimetry results demonstrate that the CZ-8 catalyst has definite micrometer scaled macroporous (0.5–5.0 μm) and interconnected mesoporous (~20 nm) structure. Raman and X-ray diffraction (XRD) results show that the dominant crystal structure of the CZ-8 is cubic fluorite and the relatively larger crystalline grain contribute to the macroporous structure construction. The filamentous diesel soot particulate (hundreds nanometers or even several micrometers) is difficult to enter the pores of the conventional mesoporous ceria-zirconia catalysts. Nonetheless, it can enter the micrometer scaled pores of the CZ-8 and hence improve the soot-catalyst contact efficiency, and oxygen can efficiently contact with soot-catalyst through the mesopores. Accordingly, the CZ-8 catalyst displays a significantly lower light-off temperature and better soot catalytic combustion performance under loose and tight contact conditions. Thus, this work suggests that enhancing solid(soot)-solid (catalyst)-gas(oxygen) contact efficiency by hierarchically porous structure with micrometer scaled macropores of catalyst is a promising new pathway for improving soot catalytic combustion performance and controlling diesel exhaust particulate emissions.

1. Introduction

Fossil fuel is the dominant energy of current world and will still dominate in the following decades despite the merging green power, such as solar and hydrogen energy [1,2]. Diesel engine plays a vital role in military, construction, agricultural equipment and transportation due to its inherent high thermal efficiency and durability [3,4]. However, environmental issues caused by the diesel exhaust emissions have been paid more and more attention hitherto [5,6]. In particular, soot from diesel combustion generally account for more than 90% of total mobile source particulate matter emissions in the atmosphere, thereby posing a significant public health risk [3,7,8]. To eliminate diesel soot emissions,

diesel particulate filter (DPF) was developed and widely applied in diesel vehicle after-treatment system nowadays, the trapping and subsequent burning of soot particles on DPF is of significance [9–11]. The operating parameters and the presence of soluble organic fractions will affect soot combustion on DPF [12,13]. However, generally, soot trapped on DPF cannot be burned spontaneously under the diesel exhaust conditions, because of high auto-ignition temperature of soot (~600 °C, and light-off temperature of ~450 °C) and low diesel exhaust temperature (200–400 °C during normal driving cycles) [14,15]. Therefore, soot combustion catalyst should be developed and loaded on DPF, and the main objective of the catalyst is to decrease the auto-ignition temperature of soot combustion [16,17]. That can make the soot

* Corresponding author.

E-mail addresses: zyang@cwnu.edu.cn (Z. Yang), huangwei.zhang@nus.edu.sg (H. Zhang).

<https://doi.org/10.1016/j.mcat.2022.112825>

Received 1 October 2022; Received in revised form 13 November 2022; Accepted 20 November 2022

Available online 28 November 2022

2468-8231/© 2022 Elsevier B.V. All rights reserved.

combustion occur under diesel exhaust temperature range and hence accelerate DPF passive regeneration.

Ceria-zirconia catalysts have been used for catalytic abatement of gasoline vehicle emission pollutants since the 1980s, which have reliable production process and mature market network [18–20]. They also are among the promising soot combustion catalyst materials because of the superior redox property and excellent soot catalytic oxidation performance [18,21,22]. Current studies indicate that suitable nanostructure can improve the soot-catalyst contact efficiency and the exposure of high active crystal planes of CeO₂ [23–25]. The controlling of electronic structure is also a viable way to improve the catalytic performance of ceria-based soot combustion catalysts [26–28]. Besides, active oxygen species amount and lattice oxygen mobility are of great significance for enhancing soot catalytic combustion [29–31]. The results from these investigations are encouraging about enhancing soot oxidation performance of ceria-based catalysts. However, decreasing the light-off temperature of soot catalytic combustion is still very challenging.

Because the soot catalytic combustion is featured by solid(soot)-solid (catalyst)-gas(O₂) reactions, the solid-solid contact efficiency of soot-catalyst is generally poor [32,33]. It leads to the high light-off temperature and poor performance of catalytic soot combustion. Therefore, it is of great importance to enhance the soot-catalyst contact efficiency for improving soot catalytic combustion performance. The diesel soot particles (~25 nm) [34,35] can evolve into particulate agglomerates through the collision and sticking [36,37], which features long filaments (generally up to >500 nm or even >1 μm) and can easily adhere to the like catalyst particles [38,39]. In our recent report [2,40,41], engineered structured (sheet, rod, etc.) ceria-based composite catalysts under micrometer/sub-micrometer scale are designed, which show a remarkably higher soot-catalyst contact efficiency and better soot catalytic combustion performance.

Besides, constructing macroporous catalyst materials is another effective way to enhance soot-catalyst contact efficiency. Recently, Wei and co-workers have developed three-dimensional ordered macroporous (3DOM) materials that obviously enhance soot-catalyst contact efficiency and soot catalytic combustion performance [42–44]. Because of the physical characteristics of the macroporous material and template, the pore size of 3DOM catalysts are generally smaller than 300 nm [42–44]. The preparation of macroporous materials with larger pore size is still highly challenging, because the excessively large pore is easy to be destroyed during the high-temperature preparation and application process. However, since the length of the soot filaments can reach hundreds of nanometers or even several micrometers, the filament-like soot particles are difficult to enter the pore of conventional porous catalyst [2,38,39].

Accordingly, the macroporous materials with larger pores, particularly with micrometer scaled macropores, should have a higher soot-catalyst contact efficiency. Moreover, hierarchically porous material is widely studied nowadays, due to its high porosity, surface area and excellent permeability. The hierarchically micrometer-scaled macroporous composite should be a promising catalyst material to enhance soot-catalyst-oxygen contact efficiency and soot catalytic combustion performance. Since the soot filaments can enter the micrometer-pore of the hierarchically micrometer-scaled macroporous catalyst, and oxygen can efficiently contact with soot-catalyst through the interconnected mesopores. Therefore, better soot catalytic combustion performance of hierarchically porous catalyst can be expected. In light of the above considerations, in this work, hierarchically porous ceria-zirconia composites with micrometer scaled macropores will be designed, and its effects on catalytic combustion of diesel soot particulates will be studied systematically.

2. Experimental method

2.1. Material preparation

All chemicals are commercially available and used without further purification. Ce(NO₃)₃•6H₂O and Zr(NO₃)₄•5H₂O are chemical pure; ethanol, lauric acid, ammonia solution and hydrogen peroxide solution are analytical reagents. The CeO₂-ZrO₂ composites were synthesized by hydrothermal process. The calculated amount of Ce(NO₃)₃•6H₂O (19.3 g) and Zr(NO₃)₄•5H₂O (8.2 g) were dissolved in an ethanol (100 mL), lauric acid (15.3 g) and water (100 mL) mixture solution, and then stirred at 50 °C for 4 h. Whereafter, the solution mixture was synchronously dropped in a beaker with 1.5% of NH₃•H₂O solution at 50 °C with efficient stirring. The pH was measured by a pH meter and controlled at 7. Then, 30% of hydrogen peroxide solution (4 mL) was dropped in the solution and kept stirring for 30 min. Afterwards, the received slurry was ripened at 180 °C for 48 h in a high-pressure autoclave. After being cooled down to room temperature, the slurry was filtered and washed by deionized water. Subsequently, the product was calcined at 600 °C for 3 h in air atmosphere, and the catalyst powder was then obtained and signed as CZ-7. All the CeO₂-ZrO₂ composite catalysts were prepared by using the same procedures, except keeping the reaction mixture solution pH value as 8, 9 and 10, respectively. The obtained CeO₂-ZrO₂ composites were marked as CZ-8, CZ-9 and CZ-10, respectively.

2.2. Materials characterization

The catalyst morphologies were observed by Zeiss MERLIN field emission scanning electron microscope (FE-SEM). Mercury porosimetry was performed on Micromeritics MicroActive AutoPore IV9500. X-ray diffraction (XRD) patterns were recorded on a PANalytical X'Pert PRO MRD X-ray powder diffractometer with Cu Kα radiation (λ = 0.15405 nm). Raman spectra were measured by using a Renishaw RM2000 laser RAMAN spectrometer with excitation wavelength of 514 nm.

Micromeritics ASAP 2020 plus physisorption apparatus was used to collect the N₂ adsorption-desorption isotherms of the catalysts at 77 K and then analyze the textural properties. All the samples were degassed at 300 °C for 3 h under vacuum before the test, and the specific surface area and pore size distribution of the catalysts were calculated by using the Brunauer-Emmett-Teller (BET) and Barret-Joyner-Halenda (BJH) equations, respectively. The mercury porosimetry test was performed on a Micromeritics MicroActive AutoPore V 9600 Mercury Porosimeter.

X-ray photoelectron spectroscopy (XPS) tests were undertaken on a Thermo Scientific Escalab 250Xi spectrometer with Al Kα source, and C 1 s at 284.8 eV was used as internal calibration. In order to minimize the photoreduction of catalyst surface elements during prolonged XPS tests [45,46], the irradiation time is less than 20 min [40,41].

Oxygen-temperature programmed desorption (O₂-TPD) performance was tested as follows. About 100 mg of the catalyst sample (20–30 mesh) was pretreated by He flow (40 mL/min) at 450 °C for 30 min in a quartz tube reactor. After being cooled down to room temperature, 5.0 vol.% O₂-He mixture (40 mL/min) was introduced at about 50 °C and kept for 1 hour. Then the gas mixture flow was changed as He flow (40 mL/min) to purge the sample until the system stabilized. At last, the quartz tube was heated to 900 °C (10 °C/min) in 40 mL/min of He flow, and the oxygen signal was monitored by TCD.

H₂ temperature-programmed reduction (H₂-TPR) test was performed on a fixed-bed dynamic adsorption apparatus. About 100 mg of the catalyst sample (20–30 mesh) was placed in a quartz reaction tube and then pretreated by N₂ flow (40 mL/min) at 450 °C for 30 min. After being cooled down to room temperature, the sample was heated up to 900 °C (10 °C/min) under 5 vol.% H₂-N₂ with a flow rate of 40 mL/min. The hydrogen consumption was detected by TCD and calibrated by pure CuO reduction.

Soot (10 mg)-catalyst (90 mg) mixture in tight contact was placed in

the fixed-bed dynamic adsorption apparatus for soot temperature-programmed reduction (soot-TPR) test. The sample was pretreated by He flow (40 mL/min) at 120 °C for 45 min, then heated up to 900 °C (10 °C/min) keeping for 1 hour under the same He flow and the soot consumption was detected by a TCD.

2.3. Catalytic performance tests

Both loose and tight contact conditions were employed to evaluate the soot catalytic abatement performances of the prepared catalysts on a fixed-bed reactor by temperature programmed combustion (TPC). About 90 mg of the catalyst was mixed with 10 mg of soot (Printex U, Degussa AG) by a spatula for 2 min so as to acquire the loose contact samples. The tight contact samples were prepared by mixing the catalyst and soot in a mortar for 5 min. For the test, 50 mL/min of N₂ flow was firstly introduced at 160 °C to pretreat the sample for 45 min in a passivated stainless-steel tubular reactor. After that, the gas flow was changed as 300 mL/min of 1000 ppm NO-10 vol.% O₂-7% steam-N₂ balance; and the reactor was heated to 600 °C (2 °C/min). The outlet CO and CO₂ concentrations were measured by a gas chromatograph (GC 126, Shanghai).

3. Results and discussion

3.1. Material characterization

3.1.1. Morphology

As shown in SEM images (Fig. 1), the morphologies of all the catalysts are irregular block-shaped agglomerations. Interestingly, the block of the CZ-8 catalyst (Fig. 1(b1)) seems porous formicary. The continuous magnification of this catalyst (Fig. 1(b2-b5)) shows that the porous structure of CZ-8 is clearly observed and the pore size is at the micrometer level. Since the Printex U soot and diesel exhaust soot particles feature agglomeration with long filaments [39,47,48] of several micrometers [38,49,50]. The soot agglomeration filaments can hardly enter the pore of the conventional mesoporous catalysts, but can feasibly enter the micrometer scaled macropores of the prepared CZ-8 catalyst. As such, compared to the other prepared catalysts, the CZ-8 catalyst should have a better contact efficiency with the soot filaments, and hence the superior catalytic soot oxidation performance of the CZ-8 can be expected.

Through magnifying the SEM field of view, it can be seen that the irregular block-shaped agglomerations of the CZ-7, CZ-8 and CZ-9

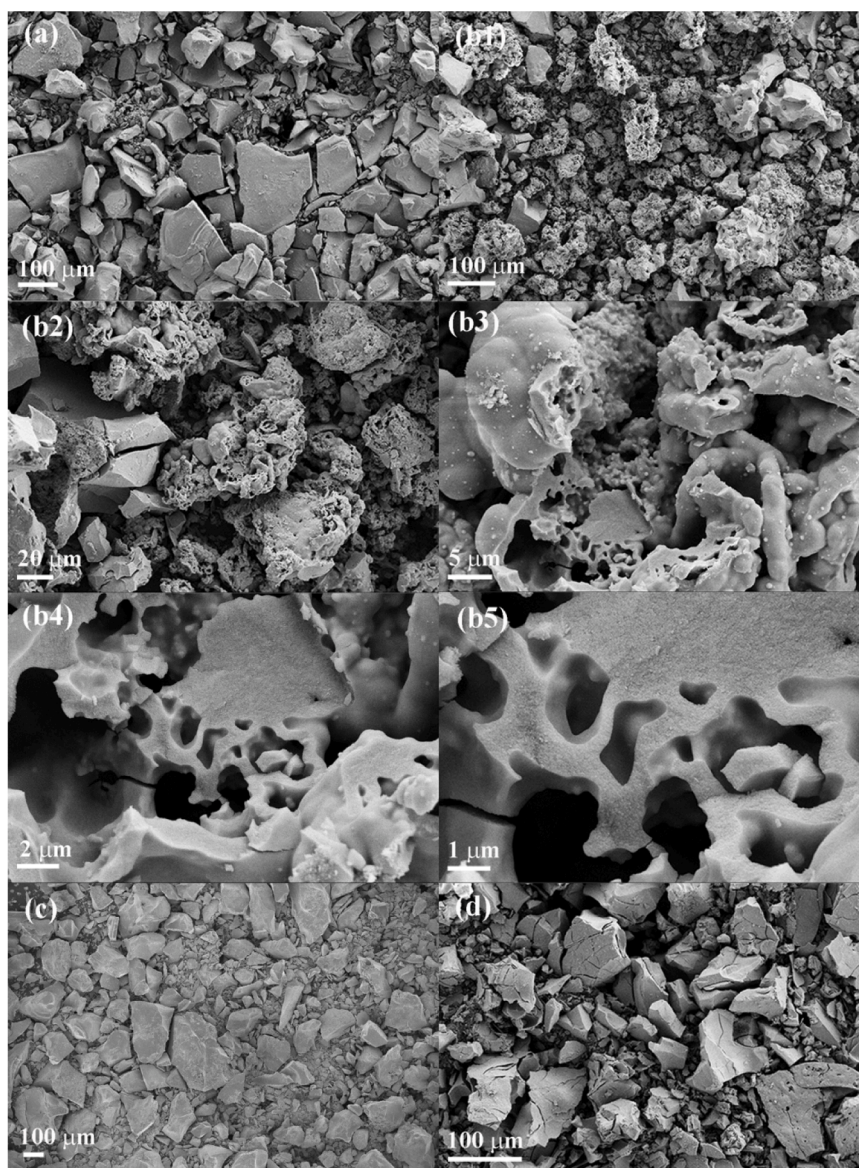


Fig. 1. SEM images of the CZ-7 (a), CZ-8 (b1-b5), CZ-9 (c) and CZ-10 (d) CeO₂-ZrO₂ composites.

samples are composed of nanoparticles (Fig. 2(a), 2(c) and 2(e)), and the interconnected nanoparticles possess many nanosized slit pores. However, for the CZ-10 catalyst, with increased pH value controlled in the preparation process, the nanoparticles are obviously aggregated and the nanosized slit pores seem not obvious. It implies that excessively high pH value would cause the destruction of the nanopores of CeO₂-ZrO₂ composites. Noteworthy, from the SEM images, the prepared CZ-8 catalyst is a hierarchically porous material. It exhibits micrometer scaled macropores that interconnected directly with nanosized slit mesopores. The presence of micro-sized pores is a significant advantage for the superior contact between solid catalyst and solid reactants (micro-sized soot agglomeration particles) as well as the particle penetration on DPF. The nanosized mesopores is beneficial for carrying oxygen throughout the soot-catalyst points. Therefore, superior soot oxidation performance of the hierarchically porous CZ-8 can be expected. To further study the textual features of the prepared CeO₂-ZrO₂ composites, N₂ adsorption-desorption technology was employed.

3.1.2. Textual features

As shown in Fig. 3(a), the CZ-7, CZ-8 and CZ-9 present a typical combination of the type H1 and H3 N₂ adsorption-desorption hysteresis

loop, which indicates that the CZ-7, CZ-8 and CZ-9 materials have plentiful slit mesopores aggregated by nanoparticles [51]. The mesoporous pore size distributions are shown in Fig. 3(b). As shown in Fig. 3 (a) insert and Fig. 3(b), the CZ-10 does not show a typical hysteresis loop, and the N₂ adsorption-desorption isotherms of the CZ-10 are characterized by the type II isotherm indicating nonpore or macroscopic pore material. This is well consistent with the SEM results.

It is noteworthy to mention that the N₂ physisorption volume of the CZ-8 at relative pressure (P/P_0) of 1.0 is approximately 580 cm³.g⁻¹, which is significantly higher than that of the CZ-7, CZ-9 and CZ-10 (78 cm³.g⁻¹, 65 cm³.g⁻¹ and 35 cm³.g⁻¹, respectively). In our previous work [41], we tested a patented product of mesoporous CeZrLaPrO_x with relatively larger pores (~80 nm). Its N₂ physisorption volume is about 340 cm³.g⁻¹, which is obviously higher than that of the conventional mesoporous ceria-zirconia composites. It indicates that the prepared CZ-8 should have significantly larger pore structure. The textual features of the prepared CeO₂-ZrO₂ composites are listed in Table 1, the pore volume of the CZ-7, CZ-8, CZ-9 and CZ-10 are 0.12 cm³.g⁻¹, 0.90 cm³.g⁻¹, 0.10 cm³.g⁻¹ and 0.05 cm³.g⁻¹, respectively. The extremely low pore volume of the CZ-10 is because the excessively high preparation pH value caused textual features destruction, which is in

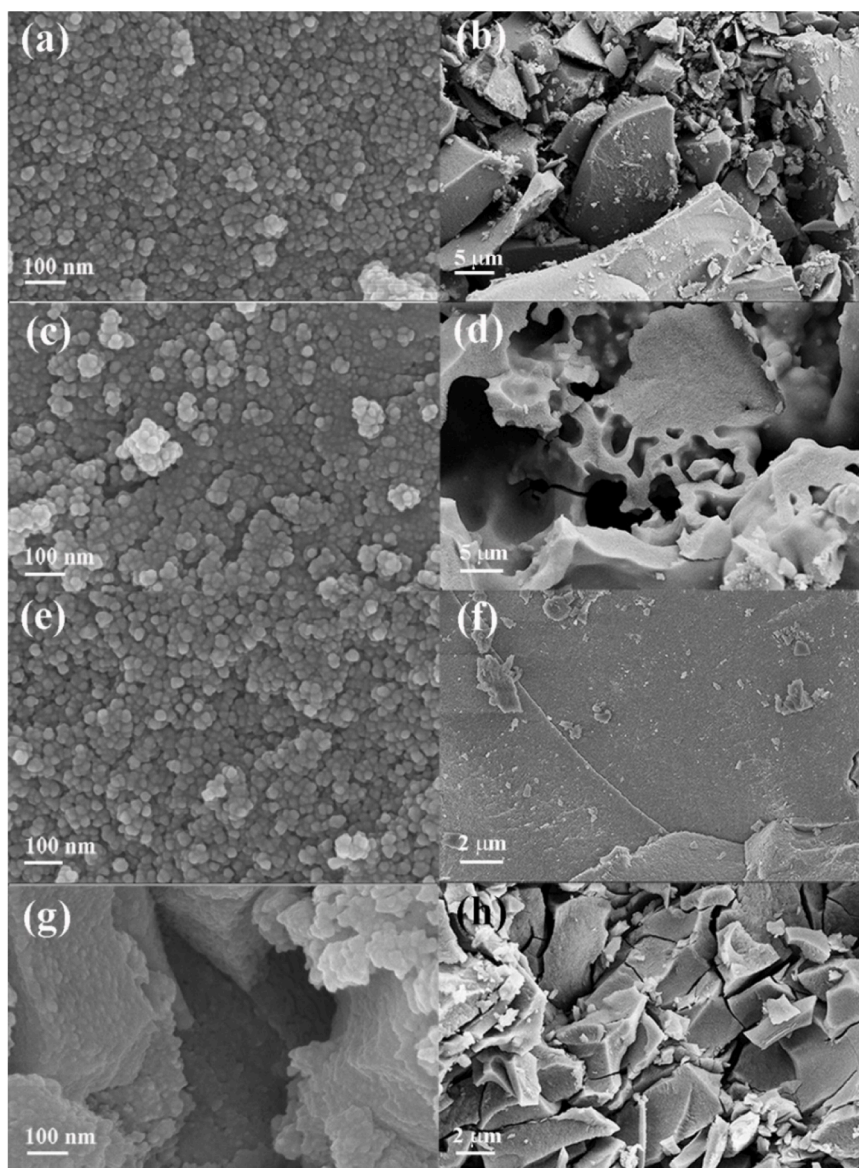


Fig. 2. SEM images of the CZ-7 (a, b), CZ-8 (c, d), CZ-9 (e, f) and CZ-10 (g, h) CeO₂-ZrO₂ composites.

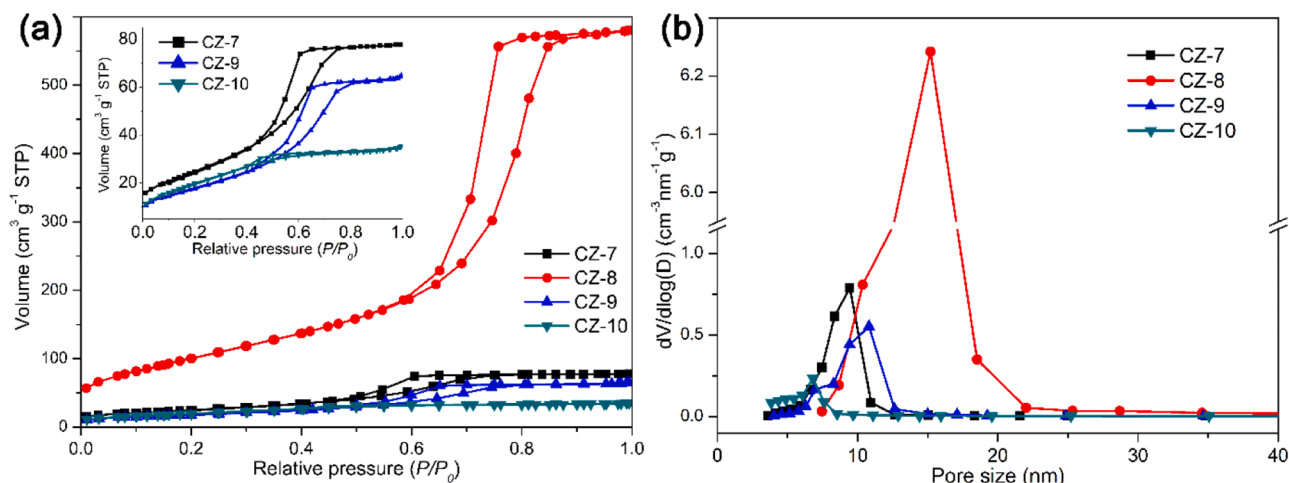


Fig. 3. N_2 adsorption-desorption isotherms of the prepared CeO_2-ZrO_2 composites.

Table 1

Textual features, structural properties and chemical states of the CeO_2-ZrO_2 composites.

Sample	Surface area ($m^2 \cdot g^{-1}$)	Pore volume ($cm^3 \cdot g^{-1}$)	Pore size (nm)	FWHM ^c (°)	Crystallite size ^c (nm)	Cell volume (nm^3)	Ce^{3+}/Ce^{4+}	O^{2-} (%)	O_2^{2-} (%)	O_2^- (%)
CZ-7	91	0.12	8.4	1.56	5.84	0.1573	0.46	70.3	17.3	12.4
CZ-8	376 ^a	0.90	14.0 ^b	0.54	11.8	0.1572	0.53	61.6	21.0	17.4
CZ-9	66	0.10	9.4	1.14	6.13	0.1571	0.56	62.0	19.2	18.8
CZ-10	74	0.05	6.2	1.72	3.54	0.1573	0.41	74.7	16.4	8.9

^a The presence of micrometer scaled macropores will affect the calculation of BET surface area;

^b N_2 adsorption-desorption is not suitable for the macroporous material of the CZ-8;

^c Measured and calculated from the XRD (111) crystal plane.

line with the foregoing SEM results. Interestingly, the CZ-8 exhibits remarkably larger pore volume than the others, by combining the results from SEM, which can ascribe to the presence of micron pores in the CZ-8 catalyst. Meanwhile, BET surface area and pore size of the CZ-8 are obviously larger than the other three (Table 1), which implies that the presence of micrometer scaled macroporous structure improved the textual features of CZ-8. However, it should be mentioned that N_2 adsorption-desorption test is not suitable for the macroporous materials (CZ-8), thus the calculation value of BET surface area of the CZ-8 should be affected by the presence of micrometer scaled macropores, and the value of pore size of the CZ-8 is not accurate. To further study the porous properties of the CZ-8, mercury porosimetry test of the CZ-8 was performed.

As shown in Fig. 4(a), the CZ-8 catalyst shows three obvious increase of cumulative pore volume at the pressure of approximately < 50 psia, 50–500 psia and $> 10,000$ psia, respectively. Generally, the pore volume at < 50 psia can be ascribed to the macroscopic pore structure constituted by the gaps of secondary particles. The pore volume at 50–500 psia is mainly associated with the macroporous structure; and the pore volume observed at $> 10,000$ psia is generally assigned to the mesoporous structure. It can be seen that the CZ-8 is a porous material with different levels pore structure. Fig. 4(b) further proves that the mesoporous and macroporous structure of CZ-8 are mainly located at < 20 nm and 0.5–5.0 μm , respectively; and the macroscopic catalyst particle gaps of CZ-8 are about $\sim 100 \mu m$. In combination with the SEM and N_2 adsorption-desorption results, it can be seen that the CZ-8 is a

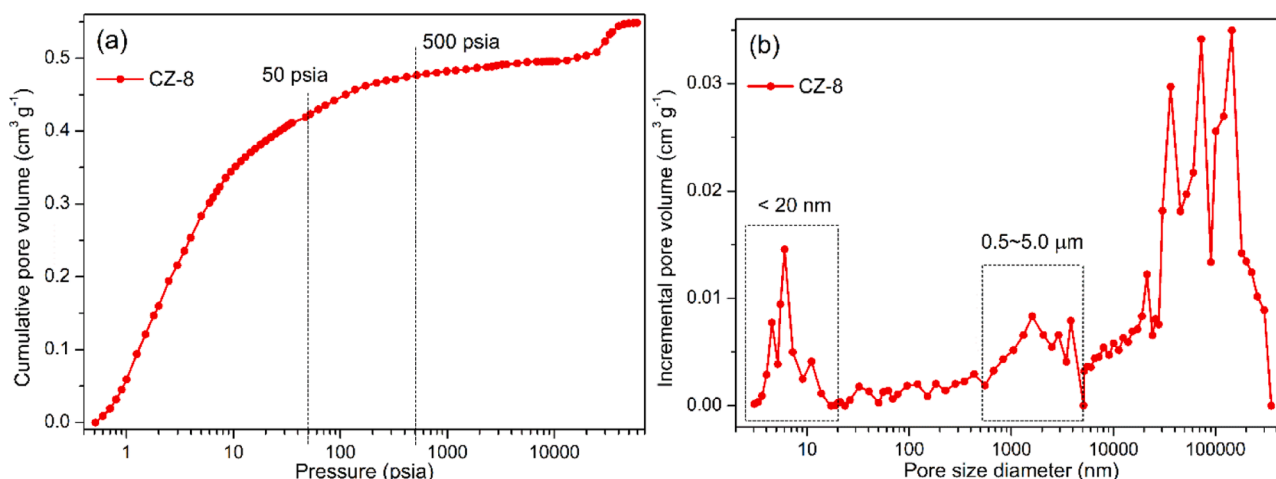


Fig. 4. Mercury porosimetry results of (a) pore volume and (b) pore size distribution of the CZ-8.

hierarchically porous composite which has micrometer scaled macroporous (0.5–5.0 μm) and interconnected mesoporous (~ 20 nm) structure. The soot filament aggregations (generally up to >500 nm or even >1 μm) can enter the micrometer scaled macropores (0.5–5.0 μm) of the CZ-8 catalyst and hence improve the soot-catalyst contact efficiency. Moreover, oxygen can contact with the soot-catalyst interfaces through the interconnected mesopores and hence promote the reaction. Therefore, the superior soot catalytic combustion performance of the hierarchically porous CZ-8 catalyst can be expected.

3.1.3. Structural properties

Fig. 5 shows the Raman spectra of the prepared $\text{CeO}_2\text{-ZrO}_2$ composites, and all the samples exhibit a strong peak at approximately 465 cm^{-1} and a weak tail peak between 550 cm^{-1} and 700 cm^{-1} . The sharp 465 cm^{-1} peak can be attributed to the F_2g mode of the cubic fluorite lattice of $\text{CeO}_2\text{-ZrO}_2$ solid solution [51–53]. The weak peak at $550\text{--}700\text{ cm}^{-1}$ is due to the structural defect (oxygen vacancy) of $\text{CeO}_2\text{-ZrO}_2$ solid solution [28,54]. The tetragonal phase characterization peaks at $200\text{--}350\text{ cm}^{-1}$ are not observed in all the samples. Thus, all the prepared $\text{CeO}_2\text{-ZrO}_2$ composites are principally cubic fluorite structure.

XRD was employed to further identify structural properties of the prepared $\text{CeO}_2\text{-ZrO}_2$ composites. As plotted in Fig. 6, all the catalysts display 2θ diffraction peaks at around 28.7° , 33.3° , 47.8° , 56.8° , 59.5° , 70.0° , 77.3° and 79.8° which fit with the (111), (200), (220), (311), (222), (400), (331) and (420) characterization peaks of the cubic $\text{Ce}_{0.8}\text{Zr}_{0.2}\text{O}_2$ solid solution (ICSD 152,477), respectively. The characterization peaks of the CZ-7 seem relatively broad, which indicates the incomplete crystallization and small crystal grain. The CZ-8 shows the sharpest XRD characterization peaks, and with the increase of synthesis pH of the $\text{CeO}_2\text{-ZrO}_2$ materials, the XRD characterization diffraction lines gradually broaden. The full width at half maximum (FWHM) of (111) facet peak of the prepared CZ-7, CZ-8, CZ-9 and CZ-10 are 1.56° , 0.54° , 1.14° and 1.72° , respectively (Table 1). The calculated crystallite sizes of the CZ-7, CZ-8, CZ-9 and CZ-10 are 5.84, 11.8, 6.13 and 3.54 nm, respectively. It can be seen that the CZ-8, synthesis pH value at approximately 8.0, showing an optimal result for crystallization in this work. The excessively low or high pH value would suppress the crystallization and crystal growth of $\text{CeO}_2\text{-ZrO}_2$ solid solution. Combined with the textual features from SEM and N_2 adsorption-desorption results, it can be inferred that the pH value of solution in synthesis system is a significant factor for the crystallization and crystal growth of $\text{CeO}_2\text{-ZrO}_2$ solid solution which can accordingly influence the crystal assembly and pore structure features.

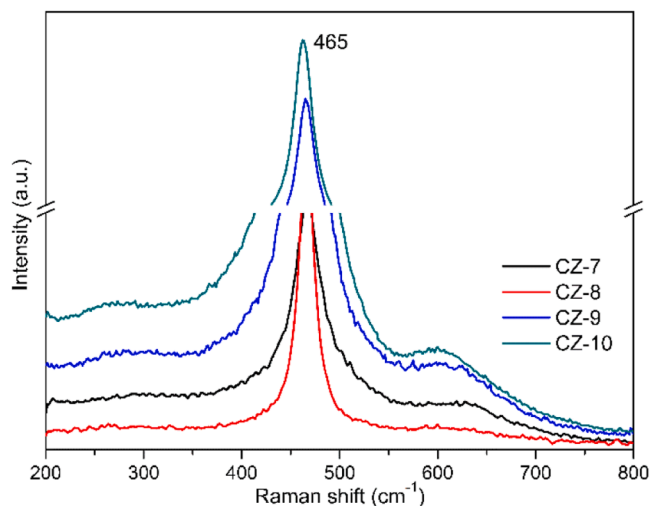


Fig. 5. Raman spectra curves of the prepared $\text{CeO}_2\text{-ZrO}_2$ composites.

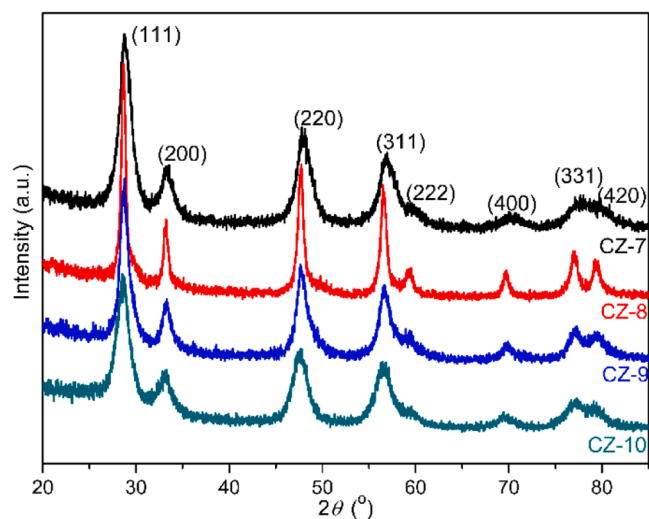


Fig. 6. XRD patterns of the prepared $\text{CeO}_2\text{-ZrO}_2$ composites.

3.1.4. Chemical states

The catalyst chemical states were analyzed by XPS measurements. As in Fig. 7(a), all the prepared catalysts show ten Ce 3d XPS characterization peaks. The peaks of $V_1\text{-}V_4$, located at around 881.2, 884.2, 899.6 and 902.6 eV, respectively, can be assigned to the Ce^{3+} species. The $U_1\text{-}U_6$ peaks at about 882.2, 888.8, 898.0, 900.8, 907.2 and 916.6 eV, respectively, are ascribed to the Ce^{4+} . The $\text{Ce}^{3+}/\text{Ce}^{4+}$ proportion is calculated by the ratio of total $V_1\text{-}V_4$ to $U_1\text{-}U_6$ peak areas [55,56]. As listed in Table 1, the $\text{Ce}^{3+}/\text{Ce}^{4+}$ proportions of the CZ-7, CZ-8, CZ-9 and CZ-10 are 0.46, 0.53, 0.56 and 0.41, respectively. It can be seen that the synthesis pH can affect the chemical states of $\text{CeO}_2\text{-ZrO}_2$ composites, excessively low or high synthesis pH is a disadvantage for generation of Ce^{3+} . The CZ-8 and CZ-9 catalysts have obviously more Ce^{3+} than the others. Since the Ce^{3+} is closely relative with the oxygen vacancy, and oxygen vacancy is a critical factor for gaseous oxygen activation to generate active oxygen species [56]. Thus, more active oxygen species and superior soot catalytic oxidation performance on the CZ-8 and CZ-9 catalysts can be expected.

The chemical states of oxygen species of the prepared $\text{CeO}_2\text{-ZrO}_2$ composites were further analyzed by XPS O1s spectra. As shown in Fig. 7(b), all the prepared catalysts show three peaks at approximately 529.3 eV, 531.2 eV and 532.3 eV, respectively, which can be ascribed to the lattice oxygen O^{2-} , chemisorbed oxygen O_2^{2-} and O_2^- , respectively [55]. The surface O_2^{2-} and O_2^- are the active oxygen species for soot catalytic oxidation reaction, that can enhance soot catalytic oxidation performance. The oxygen species ratios of the prepared $\text{CeO}_2\text{-ZrO}_2$ composites are calculated and listed in Table 1. The lattice oxygen contents of the CZ-7, CZ-8, CZ-9 and CZ-10 are 70.3%, 61.6%, 62.0% and 74.7%, respectively. Accordingly, the CZ-8 and CZ-9 catalysts have markedly more total active oxygen species (O_2^{2-} and O_2^-) than the other two. This is an advantage for the CZ-8 and CZ-9 to exhibit better catalytic soot combustion performance.

3.1.5. Redox properties

In this section, the ability to activate oxygen of the prepared catalysts was investigated by O_2 -TPD measurement. As presented in Fig. 8, all the prepared catalysts show four TPD oxygen signals. The TPD peaks located at $100\text{--}200^\circ\text{C}$ can be assigned to the desorption of weakly chemically adsorbed oxygen, which are not likely to influence the catalytic soot oxidation activity, because of the soot catalytic oxidation generally becomes higher than 250°C . The TPD signals at $450\text{--}650^\circ\text{C}$ are associated with the surface lattice oxygen that is a relevant factor for a better soot catalytic oxidation activity. The peak at higher than 650°C is associated with the bulk lattice oxygen, it is hardly to immediately participate in

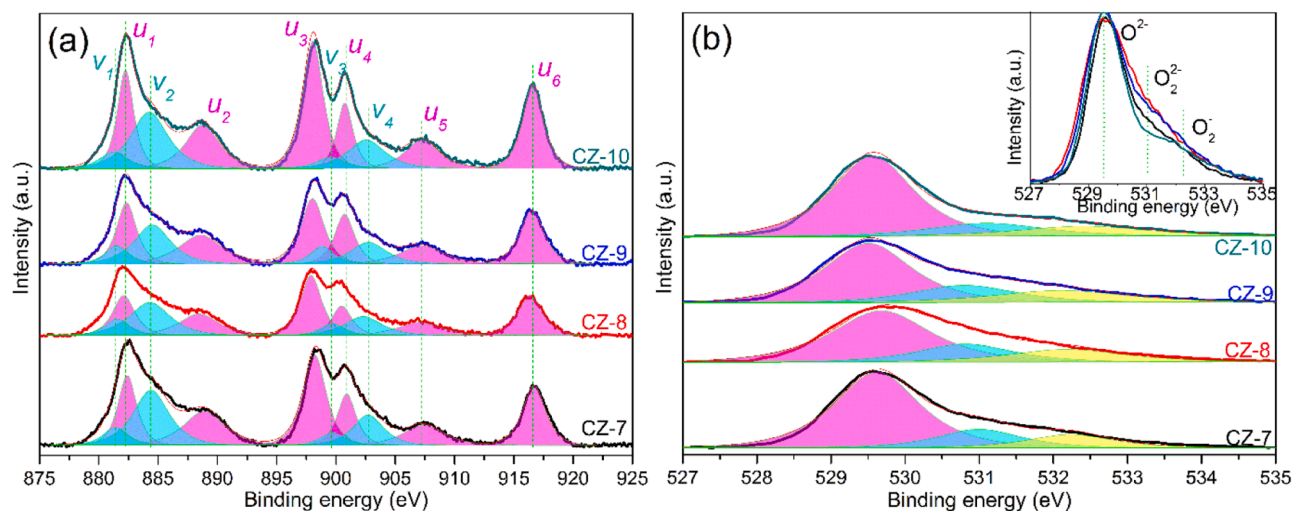


Fig. 7. XPS spectra of the prepared $\text{CeO}_2\text{-ZrO}_2$ composites: (a) Ce 3d and (b) O 1s.

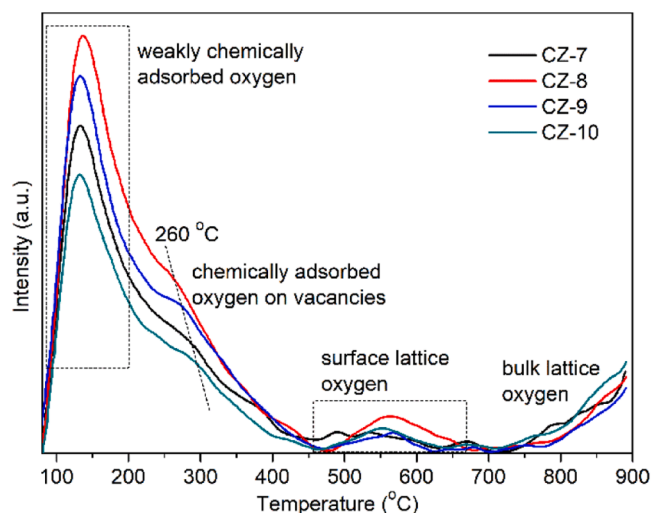


Fig. 8. O_2 -TPD curves of the prepared $\text{CeO}_2\text{-ZrO}_2$ composites.

the soot catalytic oxidation at diesel exhaust temperature range [2,41, 57]. Interestingly, the TPD signal of the chemically adsorbed oxygen on vacancies of the CZ-8 catalyst is located at approximately 260 °C, which is lower than the CZ-9, CZ-7 and CZ-10 according to priority. Besides that, the TPD peak area of the oxygen vacancies of the CZ-8 is larger than the CZ-9, CZ-7 and CZ-10 according to priority. Since oxygen vacancies are the critical factor for the activation of gaseous oxygen to generate active oxygen species. The desorption peak of oxygen vacancies of the CZ-8 shows a relatively lower temperature and larger area, which implies that the CZ-8 catalyst can supply more active oxygen at relatively lower temperature for soot oxidation. This is a favorable condition of the CZ-8 for the low-temperature soot catalytic combustion.

The redox properties of the prepared $\text{CeO}_2\text{-ZrO}_2$ composites were studied by H_2 -TPR measurement. As shown in Fig. 9, all the prepared $\text{CeO}_2\text{-ZrO}_2$ catalysts show two TPR peaks. The first peak located at below 650 °C is ascribed to the reduction of surface lattice oxygen of $\text{CeO}_2\text{-ZrO}_2$ composites, and the second peak higher than 650 °C can be assigned to the reduction of bulk lattice oxygen of $\text{CeO}_2\text{-ZrO}_2$ [20,58]. The CZ-8 catalyst shows a remarkably lower peak temperature and larger peak area of the surface lattice oxygen reduction than the others, which is because of the high surface area and superior texture property of the CZ-8 catalyst [58], this should be a huge advantage of the CZ-8 catalyst for soot catalytic combustion. The reduction peak areas and

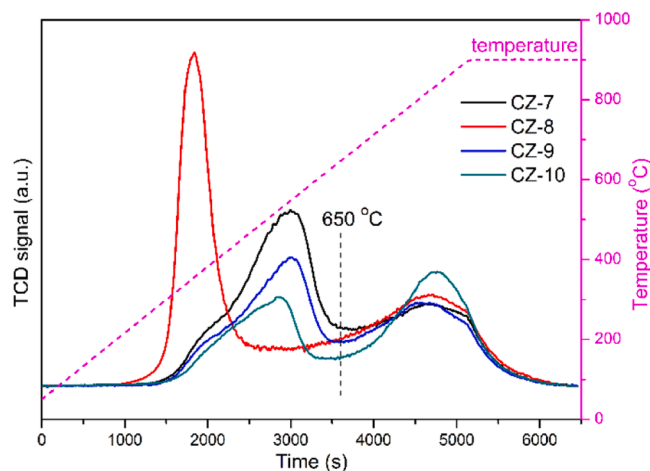


Fig. 9. H_2 -TPR curves of the prepared $\text{CeO}_2\text{-ZrO}_2$ composites.

lattice oxygen contents of the catalysts were calculated and listed in Table 2. The total lattice oxygen that can be reduced by hydrogen of the CZ-8 is about 1.562 $\text{mmol}_o/\text{g}_{\text{cat}}$, which is higher than that of the CZ-7, CZ-9 and CZ-10 (1.457, 1.182 and 1.055 $\text{mmol}_o/\text{g}_{\text{cat}}$, respectively). Specifically, the surface lattice oxygen concentration of the CZ-8 is approximately 0.948 $\text{mmol}_o/\text{g}_{\text{cat}}$, which is obviously higher than that of the CZ-7, CZ-9 and CZ-10 (0.883, 0.641 and 0.451 $\text{mmol}_o/\text{g}_{\text{cat}}$, respectively). Due to the fact that surface lattice oxygen is the active oxygen species of ceria-based catalysts for the catalytic oxidation reaction [41, 59,60], thus the CZ-8 with more surface lattice oxygen would have a superior soot catalytic combustion performance. While, although the CZ-7 catalyst has many surface lattice oxygen, the incomplete crystallization and small crystal grain (as shown in XRD results) would lead to the instability of CZ-7 catalyst during the high-temperature soot combustion reaction; hence disadvantages to the catalytic soot combustion performance. To better associate active oxygen species and soot catalytic combustion activity, soot-TPR measurement was carried out.

Fig. 10 shows the soot-TPR curves of the prepared catalysts, as can be seen that all the catalysts show two typical soot-TPR peaks at approximately 400–800 °C and higher than 800 °C, respectively. Generally, the low-temperature peak should be attributed to surface lattice oxygen reduction by soot, and the high-temperature peak can ascribe to the bulk lattice oxygen that migrate to catalyst surface and then react with soot [61,62]. Soot-TPR peak areas of the catalysts are listed in Table 2, the

Table 2
Redox properties of the CeO₂-ZrO₂ composites during the H₂-TPR and soot-TPR tests.

Catalysts	H ₂ -TPR test Area (<650 °C)	Surface lattice [O] (mmol _o /g _{cat})	Area (total)	Total lattice [O] (mmol _o /g _{cat})	Soot-TPR test Area (400–800 °C)	Area (total)
CZ-7	59,525	0.883	98,279	1.457	2114	4944
CZ-8	63,915	0.948	105,342	1.562	2974	7248
CZ-9	43,200	0.641	79,695	1.182	2012	6094
CZ-10	30,433	0.451	71,176	1.055	1514	4971

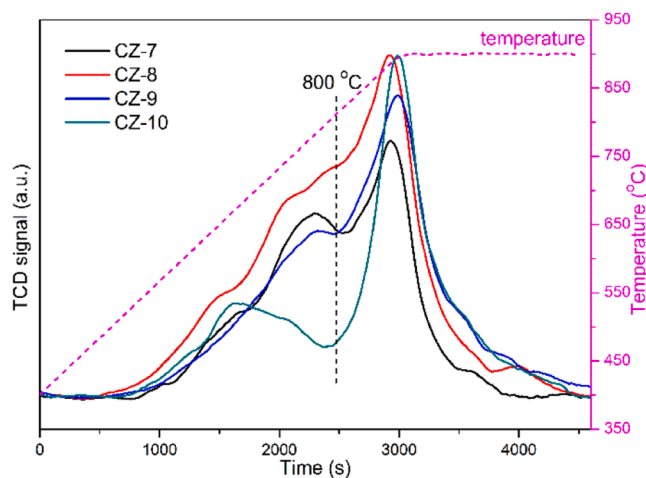


Fig. 10. Soot-TPR curves of the prepared CeO₂-ZrO₂ composites.

low-temperature peak area of CZ-8 is about 2974, which is obviously larger than that of the CZ-7, CZ-9 and CZ-10 (2114, 2012 and 1514, respectively) in sequence. This trend fits well with the H₂-TPR tests and further confirms that the surface lattice oxygen of ceria-zirconia catalyst is the active oxygen species which can play a role in soot catalytic combustion reaction.

3.2. Catalytic performance

Fig. 11 shows the catalytic performance of soot abatement on the prepared catalysts under loose contact conditions. As plotted in Fig. 11 (a), the T_p (temperature of maximum CO₂ concentration) of the CZ-7, CZ-8, CZ-9 and CZ-10 are at about 527 °C, 488 °C, 516 °C and 560 °C, respectively. Fig. 11(b) shows the soot conversion curves of the prepared

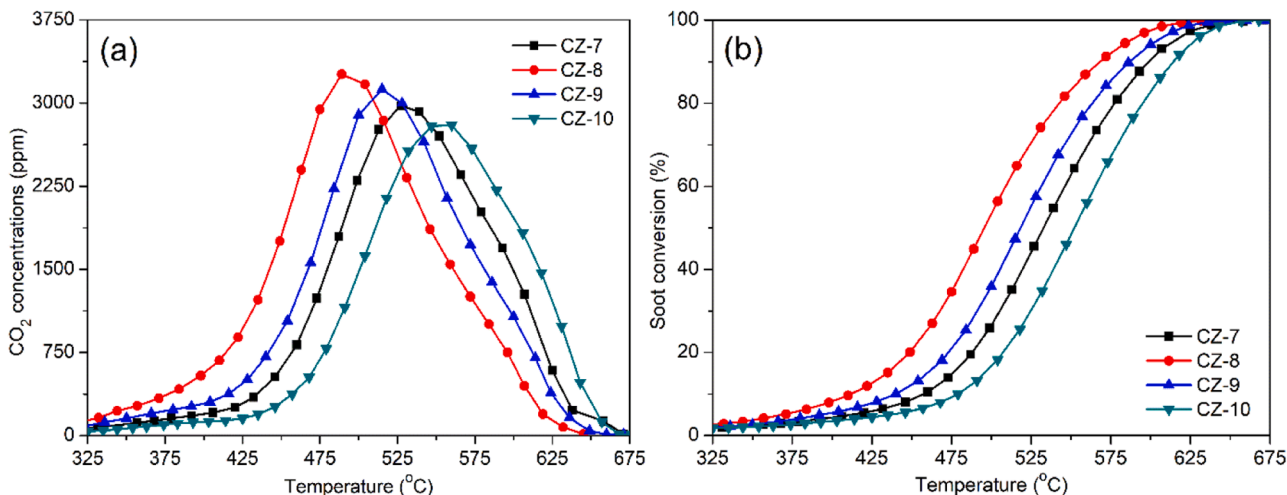


Fig. 11. Soot catalytic oxidation performance of the prepared CeO₂-ZrO₂ composites under loose contact conditions: (a) CO₂ concentrations and (b) soot conversions.

catalysts, the $T_{10\%}$ (light-off temperature), $T_{50\%}$ and $T_{90\%}$ (the temperature of soot was combusted for 10%, 50% and 90%, respectively) are presented in Table 3. The CZ-7, CZ-8, CZ-9 and CZ-10 show the $T_{10\%}$ at 458 °C, 411 °C, 439 °C and 479 °C, respectively. The $T_{50\%}$ and $T_{90\%}$ values show the similar trends with the T_p and $T_{10\%}$. Meanwhile, the reaction rates of the catalysts were calculated by the equation:

$$\text{Reaction rate} = \frac{FX}{V_m W}$$

where F is the flow rate of inlet gasses (300 mL/min), X is the molar fraction of CO₂ in ppm, V_m is the molar volume of gas (22.4 L/mol) and W is the catalyst weight. The turnover frequency (TOF) is the number of CO₂ molecules generated per active site (surface lattice oxygen) per second. As listed in Table 3, the reaction rate of the CZ-7, CZ-8, CZ-9 and CZ-10 catalysts are 1.53, 4.52, 2.35 and $0.72 \times 10^{-6} \text{ mol} \cdot \text{s}^{-1} \cdot \text{g}^{-1}$, respectively. The TOF value of the CZ-7, CZ-8, CZ-9 and CZ-10 catalysts are 1.73, 4.77, 3.67 and $1.60 \times 10^{-3} \text{ s}^{-1}$, respectively. The catalytic performance of the prepared catalysts follows the order CZ-8 > CZ-9 > CZ-7 > CZ-10. It thus can be seen that the pH value of solution in synthesis system is a relevant factor for the catalytic soot oxidation performance of CeO₂-ZrO₂ catalysts. Soot catalytic combustion performance of the CeO₂-ZrO₂ catalysts are significantly enhanced by the structure properties and particularly micrometer scaled macroporous structure.

The hierarchically porous CZ-8 catalyst, with micrometer scaled macroporous structure, shows a markedly better soot catalytic oxidation performance under tight contact conditions. It is caused by the improvement of solid(soot)-solid(catalyst) contact efficiency as reported in our recent work [2]. Because soot particulate from diesel exhaust features agglomeration with long filaments of hundreds nanometers or even several micrometers [38,41,47]. The micrometer scaled soot agglomerations are more prone to entering the micrometer scaled macropores of the catalyst rather than the nanosized pores. Therefore, the hierarchically porous CZ-8 catalyst with micrometer scaled macropores should have a higher solid(soot)-solid(catalyst) contact efficiency and

Table 3Soot catalytic oxidation data of the prepared CeO₂-ZrO₂ composites under loose and tight contact.

Catalysts	Contact	Conditions	T _p °C	T _{10%} °C	T _{50%} °C	T _{90%} °C	Reaction rate mol·s ⁻¹ ·g ⁻¹	TOF ×10 ⁻³ s ⁻¹
CZ-7	loose	this work	527	458	533	599	1.53 × 10 ^{-6a}	1.73 ^a
CZ-8	loose	this work	488	411	495	568	4.52 × 10 ^{-6a}	4.77 ^a
CZ-9	loose	this work	516	439	519	587	2.35 × 10 ^{-6a}	3.67 ^a
CZ-10	loose	this work	560	479	553	615	0.72 × 10 ^{-6a}	1.60 ^a
CZ-7	tight	this work	419	366	421	500	1.68 × 10 ^{-6b}	1.90 ^b
CZ-8	tight	this work	378	320	369	405	6.80 × 10 ^{-6b}	7.17 ^b
CZ-9	tight	this work	429	341	409	454	3.14 × 10 ^{-6b}	4.90 ^b
CZ-10	tight	this work	513	406	495	557	0.50 × 10 ^{-6b}	1.11 ^b
CeZrO ₂ (Y, La) [22]	tight	1% O ₂ -N ₂	-	302	388	450	-	-
CeZrO ₂ sheets [2]	tight	7% steam 10% O ₂ -N ₂	372	319	369	421	-	-
	loose		558	481	550	607	-	-
CeZrO ₂ sheets [2]	loose	1000 ppm NO 7% steam-10% O ₂ -N ₂	496	421	490	554	-	-
CeZrO ₂ fibers [63]	loose	21% O ₂ -N ₂	-	428	500	548	-	-
CeNiO _x 3DOM [64]	loose	500 ppm NO 5% O ₂ -N ₂	-	-	530	-	-	-

^a The reaction rate is calculated at 450 °C;^b The reaction rate is calculated at 350 °C.

hence superior catalytic soot combustion performance.

If the improvement of solid(soot)-solid(catalyst) contact efficiency, caused by the presence of micrometer scaled macropores of the CZ-8, is really responsible for the improvement of soot catalytic oxidation performance. Then, this advantage should be still effective under tight contact condition. Based on this hypothesis, soot catalytic combustion performance of the prepared catalysts under tight contact condition were tested and shown in Fig. 12. The T_p and T_{10%} of the CZ-8 are 378 °C and 320 °C, respectively, which are markedly lower than the other three; meanwhile, the reaction rate and TOF value of the CZ-8 catalyst is 6.80 × 10⁻⁶ mol·s⁻¹·g⁻¹ and 7.17 × 10⁻³ s⁻¹, which are also significantly higher than the other three catalysts. It can be seen that the trend of catalytic soot abatement performance of the prepared catalysts under tight contact condition generally agree well with the samples under loose contact condition. The presence of micrometer scaled macropore of the catalyst can significantly enhance the catalytic soot abatement performance either under loose or tight contact. Besides that, the soot catalytic combustion performance of some CeO₂-based catalysts reported by literatures [2,22,63,64] under similar conditions were listed in Table 3. It can be seen that, compared with the rare earth/transition metal elements doped CeO₂-based catalysts and nanostructured CeO₂-ZrO₂ catalysts, the CZ-8 of hierarchically micrometer-scaled macro-mesoporous CeO₂-ZrO₂ composite still shows a good catalytic soot combustion performance. Because of the soot catalytic combustion reaction on ceria-zirconia catalyst mainly follows the active oxygen (Mars-van-Krevelen) mechanism [32,64]. The surface lattice oxygen

(active oxygen species) transfer from catalyst surface to the soot surface and improve soot catalytic combustion, and then it is replenished by gaseous O₂ activation and ceria bulk lattice oxygen to surface lattice oxygen migration. The hierarchically micrometer-scaled macro-mesoporous structure of the ceria-zirconia catalysts is favor of both the gaseous O₂ activation and lattice oxygen migration (as shown in O₂-TPD and H₂/soot-TPR results). Thus, this work implies that constructing hierarchically porous structure of ceria-zirconia composites with micrometer scaled macropores is an effective method for improving diesel soot catalytic elimination performance.

4. Conclusions

In this work, we synthesize a hierarchically micrometer-scaled macro-mesoporous CeO₂-ZrO₂ composites and study its effects on catalytic combustion of diesel exhaust soot particulates. Our results show that controlling pH value of the synthesis system can affect the crystal/electron structures of the CeO₂-ZrO₂ composites, and induce the construction of micrometer-scaled macropores and mesopores. The hierarchically porous CeO₂-ZrO₂ composite with micrometer pores, CZ-8 catalyst, shows a remarkably lower light-off temperature (T_{10%}) and higher catalytic reaction rate of diesel soot catalytic combustion than the others either under tight or under loose contact condition. This is mainly caused by the micrometer pores of CZ-8 improving the soot-catalyst contact efficiency. Since the soot particulate can reach hundreds of nanometers or even several micrometers, which can hardly enter the

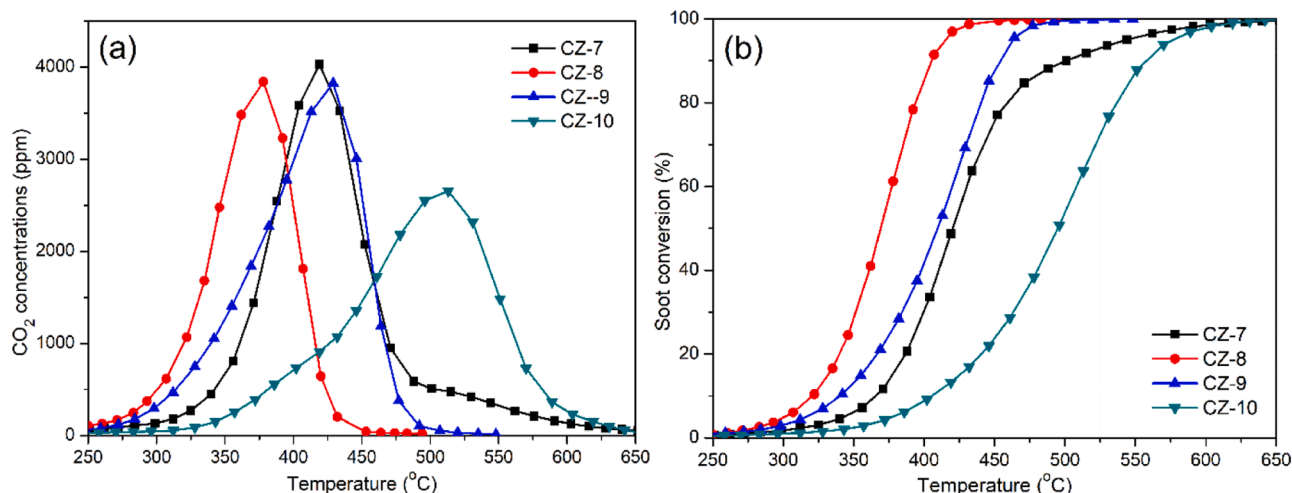


Fig. 12. CO₂ concentrations (a) and soot conversions (b) over the prepared CeO₂-ZrO₂ composites under tight contact conditions.

pore of conventional mesoporous ceria-zircon catalyst. However, soot particulate can enter the micrometer pores of the CZ-8 and hence improve the contact efficiency of soot-catalyst. Moreover, oxygen can efficiently contact the soot-catalyst interface through the interconnected mesopores of the CZ-8. The enhancement of solid(soot)-solid(catalyst)-gas(O₂) interaction is an effective way improving the catalytic performance of soot combustion. In addition, the CZ-8 has more oxygen vacancy and surface-active oxygen species (O₂²⁻ and O₂⁻), which may be another relevant factor for the enhanced catalytic performance of soot oxidation.

CRedit authorship contribution statement

Zhengzheng Yang: Investigation, Data curation, Conceptualization, Methodology, Formal analysis, Supervision, Writing – original draft. **Zhi Chen:** Validation, Data curation. **Yumeng Huang:** Investigation, Validation. **Na Zhang:** Data curation, Formal analysis. **Hunxiang Li:** Formal analysis, Resources, Project administration. **Huangwei Zhang:** Conceptualization, Formal analysis, Supervision, Writing – review & editing.

Declaration of Competing Interest

The authors declare that they have no known competing financial interests or personal relationships that could have appeared to influence the work reported in this paper.

Data Availability

Data will be made available on request.

Acknowledgements

This work was supported by the National Natural Science Foundation of China (21703174) and China West Normal University (22ka008, jgxmyb18203). The authors gratefully acknowledge Man Jiang and Chao Zeng (China West Normal University) for the experiments.

References

- [1] S. Wu, J. Akroyd, S. Mosbach, G. Brownbridge, O. Parry, V. Page, W. Yang, M. Kraft, Efficient simulation and auto-calibration of soot particle processes in Diesel engines, *Appl. Energy* 262 (2020), 114484.
- [2] Z. Yang, N. Zhang, H. Xu, Y. Li, L. Ren, Y. Liao, Y. Chen, Boosting diesel soot catalytic combustion via enhancement of solid(catalyst)-solid(soot) contact by tailoring micrometer scaled sheet-type agglomerations of CeO₂-ZrO₂ catalyst, *Combust. Flame* 235 (2022), 111700.
- [3] China Mobile Source Environmental Management Annual Report, (2021).
- [4] Z. Chen, D. Luo, H. Zhang, N. Zhang, J. Li, B. Gao, R. Qiu, Y. Li, Z. Yang, Reaction pathway of nitric oxide oxidation on nano-sized Pt/SiO₂ catalysts for diesel exhaust purification, *Mol Catal* 516 (2021), 111991.
- [5] Y. Liang, B. Zhao, J. Wang, M. Zhao, Y. Cheng, Enhanced performance of Pt-based diesel oxidation catalyst via defective MnOx: the role of Pt/MnOx interface, *Mol. Catal.* 521 (2022), 112198.
- [6] B. Gao, N. Zhang, H. Zhang, R. Qiu, Z. Chen, Y. Li, Z. Yang, Effects of platinum high-temperature redispersion on Pt/Al₂O₃ diesel oxidation catalyst for nitric oxide oxidation and its reaction pathway, *J. Environ. Chem. Eng.* 10 (2022), 108669.
- [7] C. Han, Y.C. Liu, J.Z. Ma, H. He, Key role of organic carbon in the sunlight-enhanced atmospheric aging of soot by O₂, *P. Natl. Acad. Sci. USA*, 109 (2012) 21250–21255.
- [8] J. Wei, W. Lu, Y. Zeng, H. Huang, M. Pan, Y. Liu, Physicochemical properties and oxidation reactivity of exhaust soot from a modern diesel engine: effect of oxyfuel type, *Combust. Flame* 238 (2022), 111940.
- [9] T. Andana, M. Piumetti, S. Bensaïd, N. Russo, D. Fino, Heterogeneous mechanism of NOx-assisted soot oxidation in the passive regeneration of a bench-scale diesel particulate filter catalyzed with nanostructured equimolar ceria-praseodymia, *Appl. Catal. A: Gen* 583 (2019), 117136.
- [10] A. Joshi, Review of Vehicle Engine Efficiency and Emission Control Regulations and Technologies, SAE Technical Paper, 2022-01-0540, 2022.
- [11] M.L. Godoy, V.G. Milt, E.E. Miró, E.D. Banús, Scaling-up of the catalytic stacked wire mesh filters for the abatement of diesel soot, *Catal. Today* 394-396 (2022) 434–444.
- [12] P. Pu, J. Fang, Q. Zhang, Y. Yang, Z. Qin, Z. Meng, S. Pan, Effect of operating parameters on oxidation characteristics of soot under the synergistic action of soluble organic fractions and Ash, *ACS Omega* 6 (2021) 17372–17378.
- [13] J. Fang, Z. Meng, J. Li, Y. Du, Y. Qin, Y. Jiang, W. Bai, G.G. Chase, The effect of operating parameters on regeneration characteristics and particulate emission characteristics of diesel particulate filters, *Appl. Therm. Eng.* 148 (2019) 860–867.
- [14] T. Luo, S. Liu, M. Li, W. Liu, X. Wu, S. Liu, Ozone-assisted diesel soot combustion over Mn₂O₃ catalysts: a tandem work of different reactive phases, *J. Catal.* 408 (2022) 56–63.
- [15] N.A. Sacco, J.P. Bortolozzi, V.G. Milt, E.E. Miró, E.D. Banús, Ce-Mn oxides synthesized with citric acid on ceramic papers used as diesel particulate filters, *Catal. Today* 383 (2022) 277–286.
- [16] X. Mei, X. Zhu, Y. Zhang, Z. Zhang, Z. Zhong, Y. Xin, J. Zhang, Decreasing the catalytic ignition temperature of diesel soot using electrified conductive oxide catalysts, *Nature Catal* 4 (2021) 1002–1011.
- [17] Q.L. Shi, T.Z. Liu, Q. Li, Y. Xin, X.X. Lu, W.X. Tang, Z.L. Zhang, P.X. Gao, J. A. Anderson, Multiple strategies to decrease ignition temperature for soot combustion on ultrathin MnO_{2-x} nanosheet array, *Appl. Catal. B: Environ* 246 (2019) 312–321.
- [18] A. Bueno-Lopez, Diesel soot combustion ceria catalysts, *Appl. Catal. B: Environ.* 146 (2014) 1–11.
- [19] Z.Z. Yang, Y. Yang, M. Zhao, M.C. Gong, Y.Q. Chen, Enhanced sulfur resistance of Pt-Pd/CeO₂-ZrO₂-Al₂O₃ commercial diesel oxidation catalyst by SiO₂ surface cladding, *Acta Phys-Chim Sin* 30 (2014) 1187–1193.
- [20] J. Kaspar, P. Fornasiero, M. Graziani, Use of CeO₂-based oxides in the three-way catalysis, *Catal. Today* 50 (1999) 285–298.
- [21] E. Aneghi, A. Trovarelli, Potential of Ceria-Zirconia-Based materials in carbon soot oxidation for gasoline particulate filters, *Catalysts* 10 (2020) 768.
- [22] L. Xiong, P. Yao, S. Liu, S. Li, J. Deng, Y. Jiao, Y. Chen, J. Wang, Soot oxidation over CeO₂-ZrO₂ based catalysts: the influence of external surface and low-temperature reducibility, *Mol Catal* 467 (2019) 16–23.
- [23] M.A. Stegmayer, S. Irusta, E.E. Miro, V.G. Milt, Electrospinning synthesis and characterization of nanofibers of Co, Ce and mixed Co-Ce oxides. Their application to oxidation reactions of diesel soot and CO, *Catal. Today* 383 (2022) 266–276.
- [24] B. Zhang, J. Chen, G. Wu, Y. Guo, H. Wang, Revealing the boosting role of NO for soot combustion over CeO₂(111): a first-principles microkinetic modeling, *Mol Catal* 509 (2021), 111582.
- [25] S.Q. Jian, Y.X. Yang, W. Ren, L.L. Xing, D.Y. Zhao, Y. Tian, T. Ding, X.G. Li, Kinetic analysis of morphologies and crystal planes of nanostructured CeO₂ catalysts on soot oxidation, *Chem. Eng. Sci.* 226 (2020), 115891.
- [26] Y. Yang, J. Fang, Z. Meng, P. Pu, Q. Zhang, C. Yi, S. Pan, Y. Li, Catalytic activity and influence factors of Mn-Ce mixed oxides by hydrothermal method on diesel soot combustion, *Mol. Catal.* 524 (2022), 112334.
- [27] E.J. Lee, M.J. Kim, J.W. Choung, C.H. Kim, K.Y. Lee, NOx-assisted soot oxidation based on Ag/MnOx-CeO₂ mixed oxides, *Appl. Catal. A: Gen.* 627 (2021), 118396.
- [28] Z. Yang, L. Luo, L. Tang, Z. Zhou, Z. Zhou, Y. Li, Trimesic acid assisted synthesis of cerium-manganese oxide for catalytic diesel soot elimination: enhancement of thermal aging resistibility, *Fuel* 278 (2020), 118369.
- [29] M. Cortes-Reyes, J.C. Martinez-Munuera, C. Herrera, M.A. Larrubia, L.J. Alemany, A. Garcia-Garcia, Isotopic study of the influence of oxygen interaction and surface species over different catalysts on the soot removal mechanism, *Catal. Today* 384 (2022) 33–44.
- [30] Z. Zhao, J. Ma, M. Li, W. Liu, X. Wu, S. Liu, Model Ag/CeO₂ catalysts for soot combustion: roles of silver species and catalyst stability, *Chem. Eng. J.* 430 (2022), 132802.
- [31] J.S. He, P. Yao, J. Qiu, H.L. Zhang, Y. Jiao, J.L. Wang, Y.Q. Chen, Enhancement effect of oxygen mobility over Ce_{0.5}Zr_{0.5}O₂ catalysts doped by multivalent metal oxides for soot combustion, *Fuel* 286 (2021), 119359.
- [32] B. Sellers-Anton, E. Bailon-Garcia, A. Davo-Quinonero, D. Lozano-Castello, A. Bueno-Lopez, Shaping a soot combustion Ce_{0.5}Pr_{0.5}Ox catalyst, *Appl. Surf. Sci.* 584 (2022), 152513.
- [33] T.Z. Liu, Q. Li, Y. Xin, Z.L. Zhang, X.F. Tang, L.R. Zheng, P.X. Gao, Quasi free K cations confined in hollandite-type tunnels for catalytic solid (catalyst)-solid (reactant) oxidation reactions, *Appl. Catal. B: Environ.* 232 (2018) 108–116.
- [34] X. Liang, Y. Wang, Y. Wang, B. Zhao, Z. Zhang, X. Lv, Z. Wu, X. Cai, K. Wang, Impact of lubricating base oil on diesel soot oxidation reactivity, *Combust. Flame* 217 (2020) 77–84.
- [35] B. Zhao, X. Liang, T. Li, X. Lv, S. Zhang, Impact of fuel aromatic content on soot particle physicochemical properties of marine auxiliary diesel engine, *Environ. Sci. Pollut. Res.* 29 (2022) 84936–84945.
- [36] S. Wu, C.T. Lao, J. Akroyd, S. Mosbach, W. Yang, M. Kraft, A joint moment projection method and maximum entropy approach for simulation of soot formation and oxidation in diesel engines, *Appl. Energy* 258 (2020), 114083.
- [37] M. Pan, C. Wu, W. Qian, Y. Wang, H. Huang, X. Zhou, J. Wei, Impact of dimethoxymethane-diesel fuel blends on the exhaust soot's evolutionary behavior, *Fuel* 309 (2022), 122221.
- [38] Y. Wei, J. Liu, Z. Zhao, Y. Chen, C. Xu, A. Duan, G. Jiang, H. He, Highly active catalysts of gold nanoparticles supported on three-dimensionally ordered Macroporous LaFeO₃ for soot oxidation, *Angew Chem Int Edit* 50 (2011) 2326–2329.
- [39] N. Ladommatos, H. Zhao, A guide to measurement of flame temperature and soot concentration in diesel engines using the Two-Colour method Part I: principles, SAE Technical Paper (1994), 941956.
- [40] Z. Chen, L. Chen, M. Jiang, X. Gao, M. Huang, Y. Li, L. Ren, Y. Yang, Z. Yang, Controlled synthesis of CeO₂ nanorods and their promotional effect on catalytic

- activity and aging resistibility for diesel soot oxidation, *Appl. Surf. Sci.* 510 (2020), 145401.
- [41] Z. Yang, W. Hu, N. Zhang, Y. Li, Y. Liao, Facile synthesis of ceria-zirconia solid solutions with cubic-tetragonal interfaces and their enhanced catalytic performance in diesel soot oxidation, *J. Catal.* 377 (2019) 98–109.
- [42] Y. Wei, P. Zhang, J. Xiong, Q. Yu, Q. Wu, Z. Zhao, J. Liu, SO₂-tolerant catalytic removal of soot particles over 3D Ordered Macroporous Al₂O₃-supported binary Pt–Co oxide catalysts, *Environ. Sci. Technol.* 54 (2020) 6947–6956.
- [43] J. Xiong, X. Mei, J. Liu, Y. Wei, Z. Zhao, Z. Xie, J. Li, Efficiently multifunctional catalysts of 3D ordered meso-macroporous Ce_{0.3}Zr_{0.7}O₂-supported PdAu@CeO₂ core-shell nanoparticles for soot oxidation: synergetic effect of Pd-Au-CeO₂ ternary components, *Appl. Catal. B: Environ.* 251 (2019) 247–260.
- [44] Y. Wei, J. Liu, Z. Zhao, A. Duan, G. Jiang, C. Xu, J. Gao, H. He, X. Wang, Three-dimensionally ordered macroporous Ce_{0.8}Zr_{0.2}O₂-supported gold nanoparticles: synthesis with controllable size and super-catalytic performance for soot oxidation, *Energ. Environ. Sci.* 4 (2011) 2959–2970.
- [45] P.W. Park, J.S. Ledford, Effect of crystallinity on the photoreduction of cerium oxide: A Study of CeO₂ and Ce/Al₂O₃ catalysts, *Langmuir* 12 (1996) 1794–1799.
- [46] E. Paparazzo, G.M. Ingo, N. Zacchetti, X-ray induced reduction effects at CeO₂ surfaces: an X-ray photoelectron spectroscopy study, *J. Vac. Sci. Technol. A* 9 (1991) 1416–1420.
- [47] V. Narayanaswamy, N.T. Clemens, Simultaneous LII and PIV measurements in the soot formation region of turbulent non-premixed jet flames, *P Combust. Inst.* 34 (2013) 1455–1463.
- [48] J. Wei, W. Lu, M. Pan, Y. Liu, X. Cheng, C. Wang, Physical properties of exhaust soot from dimethyl carbonate-diesel blends: characterizations and impact on soot oxidation behavior, *Fuel* 279 (2020), 118441.
- [49] R. Khobragade, S.K. Singh, P.C. Shukla, T. Gupta, A.S. Al-Fatesh, A.K. Agarwal, N. K. Labhasetwar, Chemical composition of diesel particulate matter and its control, *Catal. Rev.* 61 (2019) 447–515.
- [50] B.A. Van Setten, M. Makkee, J.A. Moulijn, Science and technology of catalytic diesel particulate filters, *Catal. Rev.* 43 (2001) 489–564.
- [51] N. Zhang, Z. Yang, Z. Chen, Y. Li, Y. Liao, Y. Li, M. Gong, Y. Chen, Synthesis of sulfur-resistant TiO₂-CeO₂ composite and its catalytic performance in the oxidation of a soluble organic fraction from diesel exhaust, *Catalysts* 8 (2018) 246.
- [52] J. Kaspar, P. Fornasiero, G. Balducci, R. Di Monte, N. Hickey, V. Sergio, Effect of ZrO₂ content on textural and structural properties of CeO₂-ZrO₂ solid solutions made by citrate complexation route, *Inorganica Chim. Acta* 349 (2003) 217–226.
- [53] P. Fornasiero, G. Balducci, R. Di Monte, J. Kaspar, V. Sergio, G. Gubitosa, A. Ferrero, M. Graziani, Modification of the redox Behaviour of CeO₂ induced by structural doping with ZrO₂, *J. Catal.* 164 (1996) 173–183.
- [54] B.M. Reddy, A. Khan, P. Lakshmanan, M. Aouine, S. Loidant, J.-C. Volta, Structural characterization of Nanosized CeO₂-SiO₂, CeO₂-TiO₂, and CeO₂-ZrO₂ catalysts by XRD, Raman, and HREM techniques, *J. Phys. Chem. B* 109 (2005) 3355–3363.
- [55] N.A. Sacco, J.P. Bortolozzi, V.G. Milt, E.E. Miró, E.D. Banús, One step citric acid-assisted synthesis of Mn-Ce mixed oxides and their application to diesel soot combustion, *Fuel* 322 (2022), 124201.
- [56] X. Mao, S. Liu, W. Liu, X. Wu, S. Liu, A simple model catalyst study to distinguish the roles of different oxygen species in propane and soot combustion, *Appl. Catal. B: Environ.* 310 (2022), 121331.
- [57] Z. Zhao, X. Yang, Y. Wu, Comparative study of Nickel-based perovskite-like mixed oxide catalysts for direct decomposition of NO, *Appl. Catal. B: Environ.* 8 (1996) 281–297.
- [58] R. Di Monte, J. Kaspar, Heterogeneous environmental catalysis - a gentle art: ceO₂-ZrO₂ mixed oxides as a case history, *Catal. Today* 100 (2005) 27–35.
- [59] L. Nie, D. Mei, H. Xiong, B. Peng, Z. Ren, X.I.P. Hernandez, A. DeLaRiva, M. Wang, M.H. Engelhard, L. Kovarik, A.K. Datye, Y. Wang, Activation of surface lattice oxygen in single-atom Pt/CeO₂ for low-temperature CO oxidation, *Science* 358 (2017) 1419–1423.
- [60] Z. Zhang, D. Han, S. Wei, Y. Zhang, Determination of active site densities and mechanisms for soot combustion with O₂ on Fe-doped CeO₂ mixed oxides, *J. Catal.* 276 (2010) 16–23.
- [61] H.L. Zhang, C.X. Zhou, M.E. Galvez, P. Da Costa, Y.Q. Chen, MnOx-CeO₂ mixed oxides as the catalyst for NO-assisted soot oxidation: the key role of NO adsorption/desorption on catalytic activity, *Appl. Surf. Sci.* 462 (2018) 678–684.
- [62] H. Liang, B. Jin, M. Li, X. Yuan, J. Wan, W. Liu, X. Wu, S. Liu, Highly reactive and thermally stable Ag/YSZ catalysts with macroporous fiber-like morphology for soot combustion, *Appl. Catal. B: Environ.* 294 (2021), 120271.
- [63] G. Yu, J. Wang, J. Liu, X. Cheng, H. Ma, H. Wu, Z. Yang, G. Zhang, X. Sun, Paper-structured catalyst based on CeO₂-ZrO₂ fibers for soot combustion, *Catal. Lett.* 149 (2019) 3543–3555.
- [64] B. Sellers-Antón, E. Bailón-García, A. Cardenas-Arenas, A. Davó-Quintero, D. Lozano-Castelló, A. Bueno-López, Enhancement of the generation and transfer of active oxygen in Ni/CeO₂ catalysts for soot combustion by controlling the Ni–Ceria contact and the three-dimensional structure, *Environ. Sci. Technol.* 54 (2020) 2439–2447.